The Apparent Constant-Phase-Element Behavior of an Ideally Polarized Blocking Electrode: A Global and Local Impedance Analysis — Source link ⌁

Vicky Mei-Wen Huang, Vincent Vivier, Mark E. Orazem, Nadine Pébère ...+1 more authors

Institutions: University of Florida, Pierre-and-Marie-Curie University, Centre national de la recherche scientifique

Topics: Constant phase element and Electrical impedance

Related papers:

- The Apparent Constant-Phase-Element Behavior of a Disk Electrode with Faradaic Reactions A Global and Local Impedance Analysis

- The Global and Local Impedance Response of a Blocking Disk Electrode with Local Constant-Phase-Element Behavior

- The analysis of electrode impedances complicated by the presence of a constant phase element

- CPE analysis by local electrochemical impedance spectroscopy

- Enhanced Graphical Representation of Electrochemical Impedance Data

Share this paper: 𝟏 🐦 in ✉

View more about this paper here: https://typeset.io/papers/the-apparent-constant-phase-element-behavior-of-an-ideally-2gvkqvjqwg

The Apparent Constant-Phase-Element Behavior of an Ideally Polarized Blocking Electrode

Vicky Mei-Wen Huang, Vincent Vivier, Mark E. Orazem, Nadine Pébère, Bernard Tribollet

The Apparent Constant-Phase-Element Behavior of an Ideally Polarized Blocking Electrode

A Global and Local Impedance Analysis

Vicky Mei-Wen Huang,[a,*] **Vincent Vivier,**[b,**] **Mark E. Orazem,**[a,***,z] **Nadine Pébère,**[c,**] **and Bernard Tribollet**[b,**]

[a]*Department of Chemical Engineering, University of Florida, Gainesville, Florida 32611, USA*
[b]*UPR15 du CNRS, Laboratoire Interfaces et Systèmes Electrochimiques, Université Pierre et Marie Curie, 75252 Paris, France*
[c]*CIRIMAT, UMR CNRS 5085, ENSIACET, 31077 Toulouse Cedex 04, France*

Two numerical methods were used to calculate the influence of geometry-induced current and potential distributions on the impedance response of an ideally polarized disk electrode. A coherent notation is proposed for local and global impedance which accounts for global, local, local interfacial, and both global and local ohmic impedances. The local and ohmic impedances are shown to provide insight into the frequency dispersion associated with the geometry of disk electrodes. The high-frequency global impedance response has the appearance of a constant-phase element (CPE) but can be considered to be only an apparent CPE because the CPE exponent α is a function of frequency.
[DOI: 10.1149/1.2398882]

Both primary and secondary current and potential distributions associated with the disk geometry have been developed by Newman.[1,2] The primary distribution applies when the current and potential are governed by the ohmic resistance to current flow in the electrolyte. The secondary distribution applies when both ohmic and kinetic resistances are controlling. In the absence of faradaic reactions and for very short time scales, the primary current distribution associated with the charging of an electrode surface can be expected to follow

$$\frac{i}{\langle i \rangle} = \frac{1}{2\sqrt{1 - \left(\dfrac{r}{r_0}\right)^2}} \qquad [1]$$

where r_0 is the radius of the disk and $\langle i \rangle$ is the average current density on the electrode. In the absence of mass-transfer limitations, the transient response of a disk electrode requires the solution of Laplace's equation with flux conditions at the electrode surface.

Nisancioglu and Newman[3,4] have developed a solution for the transient response of a faradaic reaction on a nonpolarizable disk electrode to step changes in current. The solution to Laplace's equation was performed using a transformation to rotational elliptic coordinates and a series expansion in terms of Legendre polynomials. Antohi and Scherson have recently expanded the solution to the transient problem by expanding the number of terms used in the series expansion.[5]

The solutions described above account for the relaxation of the potential at the electrode surface.[3-5] Conversely, the solution presented by Oldham[6] is incorrect because it assumes that the fixed-potential condition at the electrode surface applies for all time scales and that the local ohmic impedance is therefore a real number obtained from the primary current distribution (Eq. 1).

The impedance response of electrodes rarely show the ideal response expected for single electrochemical reactions. The impedance response typically reflects a distribution of reactivity that is commonly represented in equivalent electrical circuits as a constant phase element (CPE).[7-9] For a blocking electrode, the CPE can be represented as

$$Z(f) = R_e + \frac{1}{(j2\pi f)^\alpha Q} \qquad [2]$$

where the parameters α and Q are constants. When $\alpha = 1$, Q has units of a capacitance, i.e., $\mu F/cm^2$, and represents the capacity of the interface. When $\alpha \neq 1$, the system shows behavior that has been attributed to surface heterogeneity[10,11] or to continuously distributed time constants for charge-transfer reactions.[12-16] The phase angle associated with a CPE is independent of frequency.

Using both global and local impedance measurements on a magnesium alloy, Jorcin et al.[17] have shown that the geometry of a disk in an insulating plane can induce CPE behavior and that this CPE behavior can be associated with a radial distribution of local resistance. The authors suggested that these results could be explained in terms of the numerical and analytic treatment for the impedance response of a disk electrode presented in 1970 by Newman.[18]

The objective of this work was to explore the role of current and potential distributions on the global impedance response of an ideally polarized electrode and to relate this response to the local impedance. Subsequent papers will address the influence of current and potential distributions on the impedance response of systems exhibiting local CPE behavior[19] (i.e., coupled 2D and 3D distributions) and faradaic reactions.[20]

2D and 3D Distributions

Frequency dispersion leading to CPE behavior can be attributed to distributions of time constants along either the area of the electrode (involving only a two-dimensional surface) or along the axis normal to the electrode surface (involving a three-dimensional aspect of the electrode). A 2D distribution could arise from surface heterogeneities such as grain boundaries, crystal faces on a polycrystalline electrode, or other variations in surface properties. The frequency dispersion associated with geometry-induced nonuniform current and potential distributions results from a 2D distribution.

CPE behavior may also arise from a variation of properties in the direction that is normal to the electrode surface. Such variability may be attributed, for example, to changes in the conductivity of oxide layers[21-23] or from porosity or surface roughness.[24,25] This CPE behavior is said to arise from a 3D distribution, with the third direction being the direction normal to the plane of the electrode.[17]
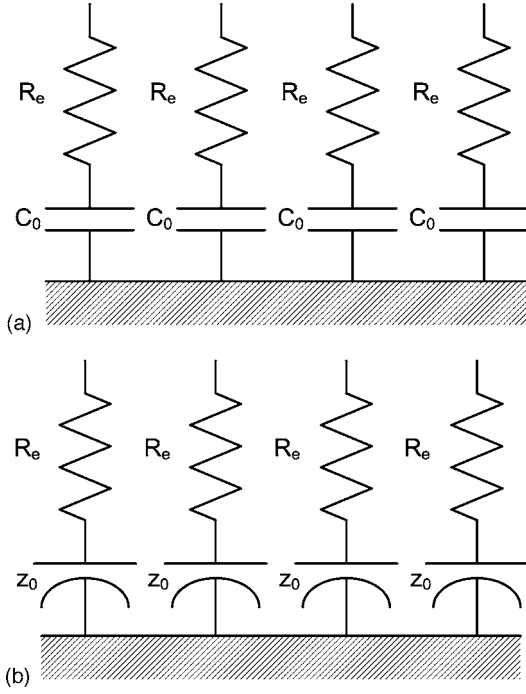
A schematic representation of a 2D distribution for an ideally polarized disk electrode is presented in Fig. 1a. For a 2D distribution, the circuit parameters, e.g., capacitance and ohmic resistance, could be a function of radial position along the electrode. Integration

Figure 1. Schematic representation of an impedance distribution for a blocking disk electrode where R_e represents the ohmic resistance, C_0 represents the interfacial capacitance, and z_0 represents an interfacial impedance corresponding to Eq. 2: (a) 2D distribution of blocking components in terms of resistors and capacitors and (b) 3D distribution of blocking components in terms of resistors and CPEs.

of the admittance associated with these circuit elements would yield a global impedance with a CPE behavior. The local impedance, in the case of a 2D distribution, would, however, show ideal behavior. A 3D distribution of blocking components in terms of resistors and constant-phase elements is presented in Fig. 1b. Such a system yields a local impedance with a CPE behavior, even in the absence of a 2D distribution of surface properties. If the 3D system shown schematically in Fig. 1b is influenced by a 2D distribution, the local impedance should reveal a variation of CPE coefficients along the surface of the electrode. Thus, local impedance measurements can be used to distinguish whether the CPE behavior arises from a 2D distribution, from a 3D distribution, or from a combined 2D and 3D distribution.

Using both global and local impedance measurements on a disk made of AZ91 magnesium alloy, Jorcin et al.[17] found CPE behavior that was attributed to a 2D distribution, which yielded locally a pure capacitive response coupled with a radial distribution of local resistance. Jorcin et al.[17] have also found CPE behavior on a pure aluminum disk in which the local impedance response showed a CPE which was modified only slightly by an apparent 2D distribution.

Mathematical Development

The steady-state solution for the current distribution at a blocking electrode is that the current is equal to zero. The primary current distribution given as Eq. 1 therefore applies, not at the steady state, but at infinite frequency. This situation differs from the special case of a faradaic system with an ohmic resistance that is much larger than the kinetic resistance and for which Eq. 1 provides the steady-state current distribution.

The object of this work was to calculate, from first principles, the influence of geometry-induced current and potential distributions on the impedance response of a disk electrode. The mathematical development follows that presented by Newman.[18] Laplace's equation in cylindrical coordinates was expressed in rotational elliptic coordinates, i.e.

$$y = r_0 \xi \eta \qquad [3]$$

and

$$r = r_0 \sqrt{(1 + \xi^2)(1 - \eta^2)} \qquad [4]$$

where $0 \leq \xi \leq \infty$ and $0 \leq \eta \leq 1$. Within the revised coordinate system, the electrode surface at $y = 0$ and $r \leq r_0$ can be found at $\xi = 0$ and $0 \leq \eta \leq 1$. The reference electrode and counter electrode located at $r \to \infty$ can be found at $\xi \to \infty$. The insulating surface of the disk at $y = 0$ and $r > r_0$ is located at $\eta = 1$ and $0 < \xi \leq \infty$, and the center line at $y > 0$ and $r = 0$ is located at $\eta = 0$ and $0 < \xi \leq \infty$.

Laplace's equation can be expressed in rotational elliptic coordinates as

$$\frac{\partial}{\partial \xi}\left[(1 + \xi^2)\frac{\partial \Phi}{\partial \xi}\right] + \frac{\partial}{\partial \eta}\left[(1 - \eta^2)\frac{\partial \Phi}{\partial \eta}\right] = 0 \qquad [5]$$

The potential was separated into steady and time-varying parts as

$$\Phi = \bar{\Phi} + \mathrm{Re}[\tilde{\Phi}\exp(j\omega t)] \qquad [6]$$

where $\bar{\Phi}$ is the steady-state solution for potential and $\tilde{\Phi}$ is the complex oscillating potential. Thus, Eq. 5 could be written as

$$2\xi\frac{\partial \tilde{\Phi}_r}{\partial \xi} + (1 + \xi^2)\frac{\partial^2\tilde{\Phi}_r}{\partial \xi^2} - 2\eta\frac{\partial \tilde{\Phi}_r}{\partial \eta} + (1 - \eta^2)\frac{\partial^2\tilde{\Phi}_r}{\partial \eta^2} = 0 \qquad [7]$$

and

$$2\xi\frac{\partial \tilde{\Phi}_j}{\partial \xi} + (1 + \xi^2)\frac{\partial^2\tilde{\Phi}_j}{\partial \xi^2} - 2\eta\frac{\partial \tilde{\Phi}_j}{\partial \eta} + (1 - \eta^2)\frac{\partial^2\tilde{\Phi}_j}{\partial \eta^2} = 0 \qquad [8]$$

where $\tilde{\Phi}_r$ and $\tilde{\Phi}_j$ refer to the real and imaginary parts of the complex oscillating potential, respectively.

The flux boundary condition at the electrode surface ($\xi = 0$ and $0 \leq \eta \leq 1$) is

$$i = C_0\frac{\partial (V - \Phi_0)}{\partial t} = -\kappa\left.\frac{\partial \Phi}{\partial y}\right|_{y=0} = -\frac{\kappa}{r_0 \eta}\left.\frac{\partial \Phi}{\partial \xi}\right|_{\xi=0} \qquad [9]$$

where C_0 is the interfacial capacitance and κ is the electrolyte conductivity. Equation 9 was written in frequency domain as

$$K\tilde{\Phi}_j = -\frac{1}{\eta}\left.\frac{\partial \tilde{\Phi}_r}{\partial \xi}\right|_{\xi=0} \qquad [10]$$

and

$$K\tilde{V}_r - K\tilde{\Phi}_r = -\frac{1}{\eta}\left.\frac{\partial \tilde{\Phi}_j}{\partial \xi}\right|_{\xi=0} \qquad [11]$$

where $\tilde{V}_r$ represents the imposed perturbation in the electrode potential referenced to an electrode at infinity and K is the dimensionless frequency

$$K = \frac{\omega C_0 r_0}{\kappa} \qquad [12]$$

At $\eta = 0$ and $\eta = 1$, for all $\xi > 0$, zero-flux conditions impose that

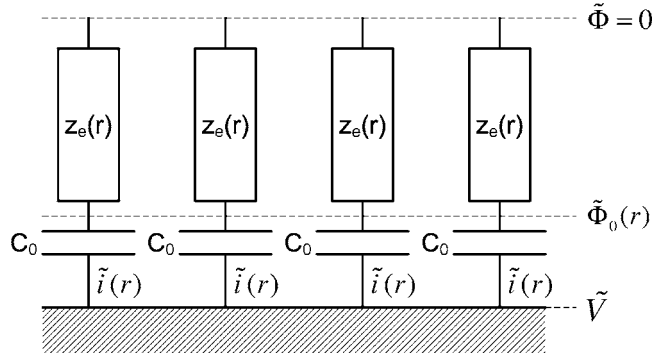$$\frac{\partial \tilde{\Phi}_r}{\partial \eta} = 0 \qquad [13]$$

and

$$\frac{\partial \tilde{\Phi}_j}{\partial \eta} = 0 \qquad [14]$$

At the far boundary condition ($\xi \to \infty$ and $0 \leq \eta \leq 1$)

$$\tilde{\Phi}_r = 0 \qquad [15]$$

and

Figure 2. The location of current and potential terms that make up definitions of global and local impedance.

$$\tilde{\Phi}_j = 0 \qquad [16]$$

The equations were solved under the assumption of a uniform capacitance C_0 using the collocation package PDE2D developed by Sewell.[26] Calculations were performed for differing domain sizes, and the results reported here were obtained by extrapolation to an infinite domain size.

The equations were also solved in the cylindrical coordinates using a finite-elements package FEMLAB. The results obtained by the two packages were in excellent agreement for dimensionless frequencies $K < 100$.

Definition of Terms

The global impedance results presented in the following section can be understood through examination of the local impedance distribution. As there are several types of local impedance at play, discussion of local impedance requires clear notation and definitions.

A schematic representation of the electrode–electrolyte interface is given as Fig. 2, where the block used to represent the local ohmic impedance reflects the complex character of the ohmic contribution to the local impedance response. The impedance definitions presented in Table I differ in the potential and current used to calculate the impedance. To avoid confusion with local impedance values, the symbol y is used to designate the axial position in cylindrical coordinates.

Global impedance.— The global impedance is defined to be

$$Z = \frac{\tilde{V}}{\tilde{I}} \qquad [17]$$

where the complex current contribution is given by

$$\tilde{I} = \int_0^{r_0} \tilde{i}(r) 2\pi r dr \qquad [18]$$

The use of an upper-case letter signifies that Z is a global value. The global impedance may have real and imaginary values designated as Z_r and Z_j, respectively. The total current could also be represented by $\tilde{I} = \pi r_0^2 \langle \tilde{i}(r) \rangle$, where the brackets signify the area-average of the current density.

Local impedance.— The term local impedance traditionally involves the potential of the electrode measured relative to a reference electrode far from the electrode surface.[27,28] Thus, the local impedance is given by

Table I. Notation proposed for local impedance variables.

Symbol	Meaning	Units
Z	global impedance (Eq. 17)	Ω or Ω cm^2
Z_r	real part of global impedance	Ω or Ω cm^2
Z_j	imaginary part of global impedance	Ω or Ω cm^2
Z_0	global interfacial impedance (Eq. 24)	Ω or Ω cm^2
$Z_{0,r}$	real part of global interfacial impedance	Ω or Ω cm^2
$Z_{0,j}$	imaginary part of global interfacial impedance	Ω or Ω cm^2
Z_e	global ohmic impedance (Eq. 26)	Ω or Ω cm^2
$Z_{e,r}$	real part of global ohmic impedance	Ω or Ω cm^2
$Z_{e,j}$	imaginary part of global ohmic impedance	Ω or Ω cm^2
z	local impedance (Eq. 19)	Ω cm^2
z_r	real part of local impedance	Ω cm^2
z_j	imaginary part of local impedance	Ω cm^2
z_0	local interfacial impedance (Eq. 21)	Ω cm^2
$z_{0,r}$	real part of local interfacial impedance	Ω cm^2
$z_{0,j}$	imaginary part of local interfacial impedance	Ω cm^2
z_e	local ohmic impedance (Eq. 22)	Ω cm^2
$z_{e,r}$	real part of local ohmic impedance	Ω cm^2
$z_{e,j}$	imaginary part of local ohmic impedance	Ω cm^2
$\langle \Phi \rangle$	spatial average of potential	V
$\bar{\Phi}$	time average or steady-state value of potential	V
$\langle i \rangle$	spatial average of current density	A/cm^2
$\bar{i}$	time average or steady-state value of current density	A/cm^2
y	axial position variable	cm

$$z = \frac{\tilde{V}}{\tilde{i}(r)} \qquad [19]$$

The use of a lower-case letter signifies that z is a local value. The local impedance may have real and imaginary values designated as z_r and z_j, respectively.

The global impedance can be expressed in terms of the local impedance as

$$Z = \left\langle \frac{1}{z} \right\rangle^{-1} \qquad [20]$$

Equation 20 is consistent with the treatment of Brug et al.[7] in which the admittance of the disk electrode was obtained by integration of a local admittance over the area of the disk.

Local interfacial impedance.— The local interfacial impedance involves the potential of the electrode measured relative to a reference electrode $\Phi_0(r)$ located at the outer limit of the diffuse double layer. Thus, the local interfacial impedance is given by

$$z_0 = \frac{\tilde{V} - \tilde{\Phi}_0(r)}{\tilde{i}(r)} \qquad [21]$$

The use of a lower-case letter again signifies that z_0 is a local value, and the subscript 0 signifies that z_0 represents a value associated only with the surface. The local interfacial impedance may have real and imaginary values designated as $z_{0,r}$ and $z_{0,j}$, respectively.

Local ohmic impedance.— The local ohmic impedance involves the potential of a reference electrode $\tilde{\Phi}_0(r)$ located at the outer limit of the diffuse double layer and the potential of a reference electrode located far from the electrode $\tilde{\Phi}(\infty) = 0$ (see Fig. 2). Thus, the local ohmic impedance is given by

$$z_e = \frac{\tilde{\Phi}_0(r)}{\tilde{i}(r)} \qquad [22]$$

The use of a lower-case letter again signifies that z_e is a local value, and the subscript e signifies that z_e represents a value associated only with the ohmic character of the electrolyte. The local ohmic

impedance may have real and imaginary values designated as $z_{e,r}$ and $z_{e,j}$, respectively. The local impedance

$$z = z_0 + z_e \qquad [23]$$

can be represented by the sum of local interfacial and local ohmic impedances.

The representation of an ohmic impedance as a complex number represents a departure from standard practice, and the related insights constitute a major contribution of the present work. As is shown in subsequent sections, the local impedance has inductive features that are not seen in the local interfacial impedance. As the calculations assumed an ideally polarized blocking electrode, the result is not influenced by faradaic reactions and can be attributed only to the ohmic contribution of the electrolyte.

Global interfacial impedance.— The global interfacial impedance is defined to be

$$Z_0 = 2\pi \left(\int_0^{r_0} \frac{1}{z_0(r)} r dr \right)^{-1} \qquad [24]$$

or

$$Z_0 = \left\langle \frac{1}{z_0(r)} \right\rangle^{-1} \qquad [25]$$

The use of an upper-case letter signifies that Z_0 is a global value. The global interfacial impedance may have real and imaginary values designated as $Z_{0,r}$ and $Z_{0,j}$, respectively.

Global ohmic impedance.— The global ohmic impedance is defined to be

$$Z_e = Z - Z_0 \qquad [26]$$

The use of an upper-case letter signifies that Z is a global value. As is shown in subsequent sections, the global ohmic impedance has a complex behavior in a mid-frequency range (near $K = 1$). The global ohmic impedance may have real and imaginary values designated as $Z_{e,r}$ and $Z_{e,j}$, respectively.

Results and Discussion

The calculated results for global, local, local interfacial, and both local and global ohmic impedances are presented in this section. The results of both the collocation and finite element method (FEM) methods were in perfect agreement for frequencies $K < 100$.

Global impedance.— The global impedance response presented in Fig. 3a shows the influence of frequency dispersion at frequencies $K > 1$. This dispersion is seen as a deviation from the vertical line obtained for low frequencies ($K < 1$). The expanded logarithmic representation presented in Fig. 3b shows the agreement with the numerical solutions presented by Newman.[18] The impedance is made dimensionless according to $Z\kappa/r_0\pi$, in which the units of impedance Z are scaled by unit area, for example, Ω cm^2.

The comparison with Newman's calculations is seen more clearly in the representation of the real and imaginary parts of the impedance response shown in Fig. 4a and b, respectively. As discussed by Orazem et al.,[29] the change in the slope of the lines presented in Fig. 4b shows that the impedance response transitions from ideal RC behavior at low frequencies to a CPE-like behavior at frequencies $K > 1$. The slope is equal to $-\alpha$, the exponent of the CPE presented in Eq. 2. A deviation from Newman's results is seen for both the collocation and FEM calculations for frequencies $K > 100$. This error is attributed to a singular perturbation problem that arises at the periphery of the electrode at high frequencies.[18]

The value of $-\alpha$, which is equal to the slope of the $\log(Z_j\kappa/r_0\pi)$ with respect to $\log(K)$, is presented in Fig. 5 as a function of dimensionless frequency K. The numerical results obtained by collocation and FEM methods is compared to the asymptotic limit developed by Newman using a singular perturbation approach. The system behaves as an ideal capacitor at low frequencies $K < 1$ with $\alpha = 1$. At

(a)

(b)
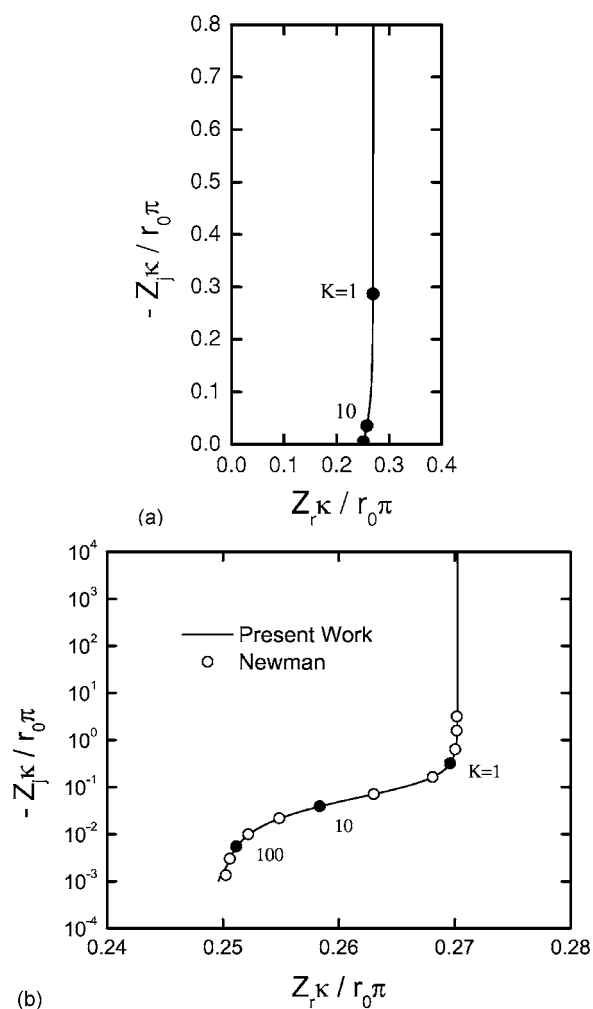
Figure 3. Calculated Nyquist representation of the impedance response for an ideally polarized disk electrode: (a) linear plot showing effect of dispersion at frequencies $K > 1$ as a deviation from a vertical line and (b) logarithmic scale showing agreement with the calculations of Newman.

frequencies $K > 1$, the value of alpha changes to roughly $\alpha = 0.85$ before beginning a gradual return towards unity. As the slope is not independent of frequency, the frequency dispersion seen at $K > 1$ does not represent true CPE behavior.

The frequency $K = 1$ at which the current and potential distributions begin to influence the impedance response can be expressed as

$$f = \frac{\kappa}{2\pi C_0 r_0} \qquad [27]$$

or, in terms of electrolyte resistance, as

$$f = \frac{1}{8 C_0 R_e} \qquad [28]$$

As shown in Fig. 6, this characteristic frequency can be well within the range of experimental measurements. The value $\kappa/C_0 = 10^4$ cm/s can be obtained for a capacitance $C_0 = 1$ μF/cm^2 (corresponding to an oxide layer) and conductivity $\kappa = 0.01$ S/cm (corresponding to a 0.1 M NaCl solution). The value $\kappa/C = 10^3$ cm/s can be obtained for a capacitance $C_0 = 10$ μF/cm^2 (corresponding to the double layer on an inert metal electrode) and conductivity $\kappa = 0.01$ S/cm (corresponding to a 0.1 M NaCl solution). Figure 6 can be used to show that, by using an electrode that is sufficiently small, the experimentalist may be able to avoid the frequency range that is influenced by current and potential distributions.
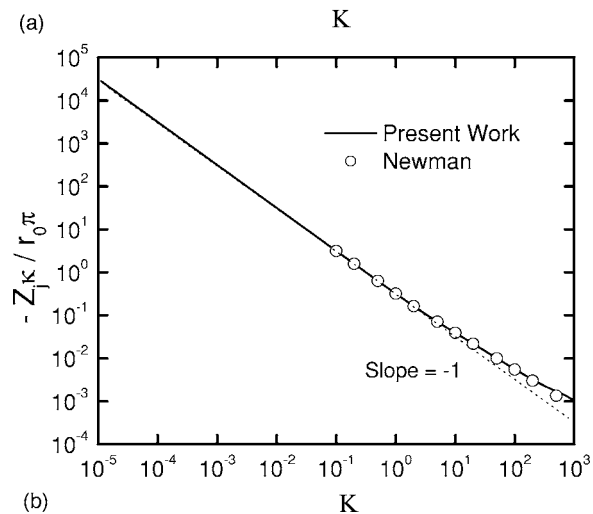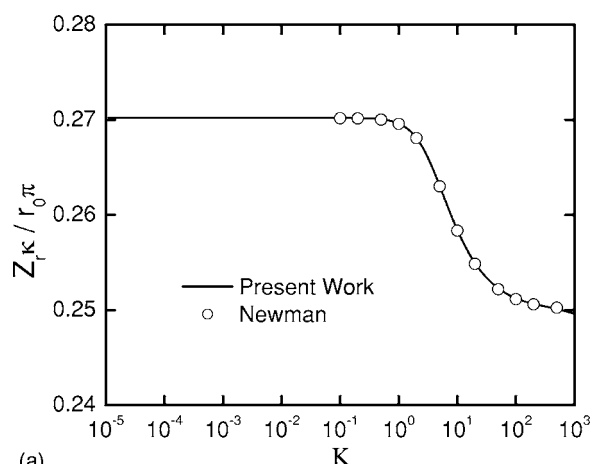
Figure 4. Calculated representation of the impedance response for an ideally polarized disk electrode: (a) real part and (b) imaginary part showing agreement with the calculations and asymptotic formula of Newman.

Local interfacial impedance.— The calculated local interfacial impedance is presented in Fig. 7a as a function of frequency with position as a parameter and in Fig. 7b as a function of position with
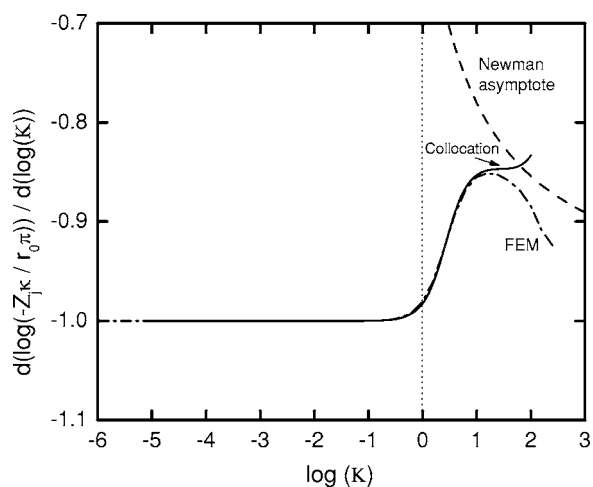

Figure 5. The slope of $\log(Z_j\kappa/r_0\pi)$ with respect to $\log(K)$ (Fig. 4b) as a function of $\log(K)$. The results were calculated by the collocation method, by FEM methods, and by using the asymptotic formula of Newman. The value of this slope is equal to $-\alpha$.
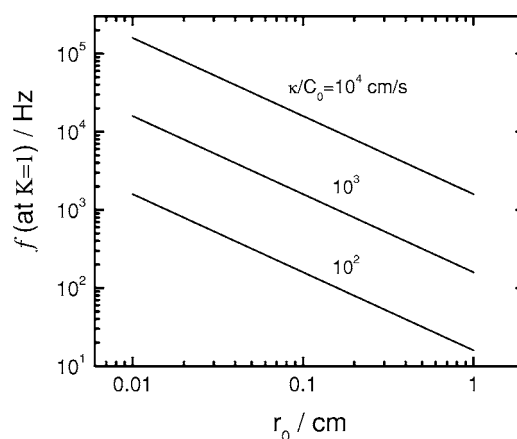

Figure 6. The frequency $K = 1$ at which the current distribution influences the impedance response with κ/C_0 as a parameter.

frequency as a parameter. All four curves indicated in Fig. 7a and b, respectively, are superposed. The results presented in Fig. 7 show that the local interfacial impedance is that associated with a pure capacitive behavior. At all frequencies, $z_{0,j}\kappa K/r_0\pi = 1/\pi$ as is expected for an ideal capacitance. The real part of the local interfacial impedance, not shown here, was equal to zero within computational accuracy.
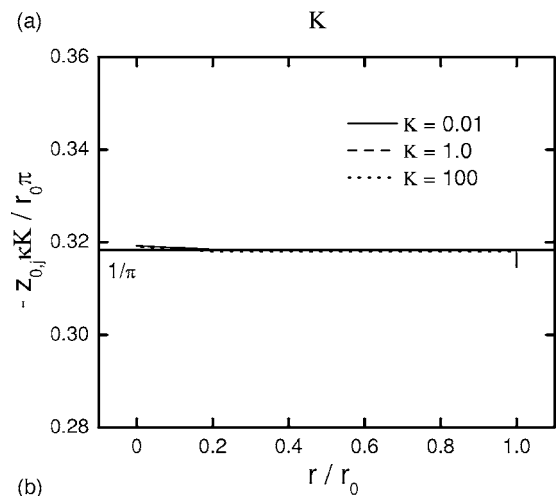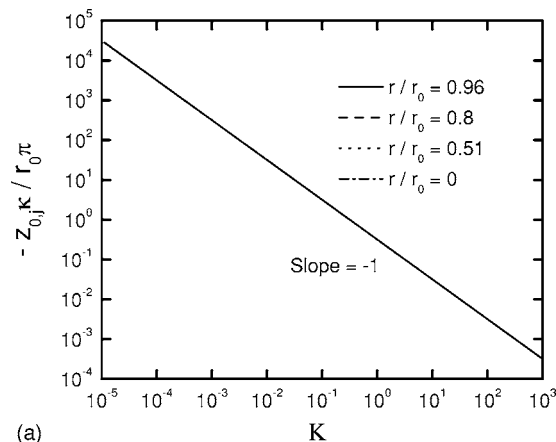
Figure 7. Calculated imaginary part of the local interfacial impedance: (a) as a function of frequency with position as a parameter and (b) as a function of position with frequency as a parameter. All four curves indicated in Fig. 7a and b, respectively, are superposed.
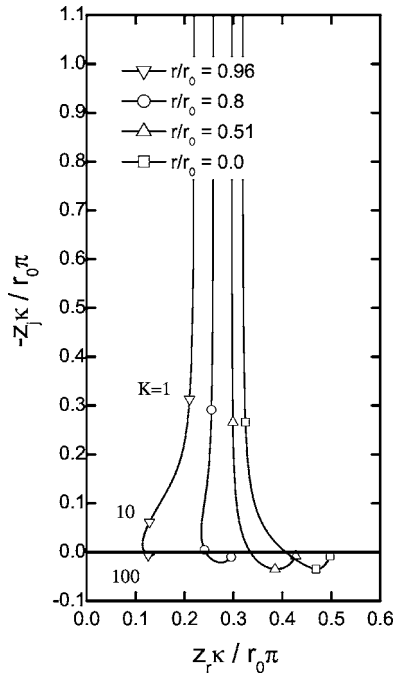
Figure 8. The local impedance in Nyquist format with radial position as a parameter.

Figure 9. Calculated local impedance with radial position as a parameter: (a) real part and (b) imaginary part.

Local impedance.— The calculated local impedance response is presented in Fig. 8 in Nyquist format with radial position as a parameter. The dimensionless impedance is scaled to the disk area πr_0^2 in order to show the comparison with the asymptotic value of 0.25 for the real part of the dimensionless impedance. The impedance is largest at the center of the disk and smallest at the periphery, reflecting the greater accessibility of the periphery of the disk electrode. Inductive loops are seen at high frequencies, and these were obtained by both methods of calculation.

The real and imaginary parts of the local impedance are presented in Fig. 9a and b, respectively, with radial position as a parameter. The real part of the local impedance presented in Fig. 9a reaches asymptotic values at $K \to 0$ and $K \to \infty$. The imaginary part presented in Fig. 9b shows the change of sign associated with the inductive features seen in Fig. 8. The changes in sign occur at frequencies well below $K = 100$, showing that the inductive loop cannot be ascribed to a calculation artifact. The deviation from ideal capacitive behavior for frequencies $K > 1$ is similar to that seen in Fig. 4b for the imaginary part of the global impedance.

The radial distribution of the real and imaginary impedance is presented in Fig. 10a and b, respectively, with dimensionless frequency K as a parameter. At high frequencies, e.g., $K = 100$, the calculated radial distribution of the real part of the local impedance follows the expression
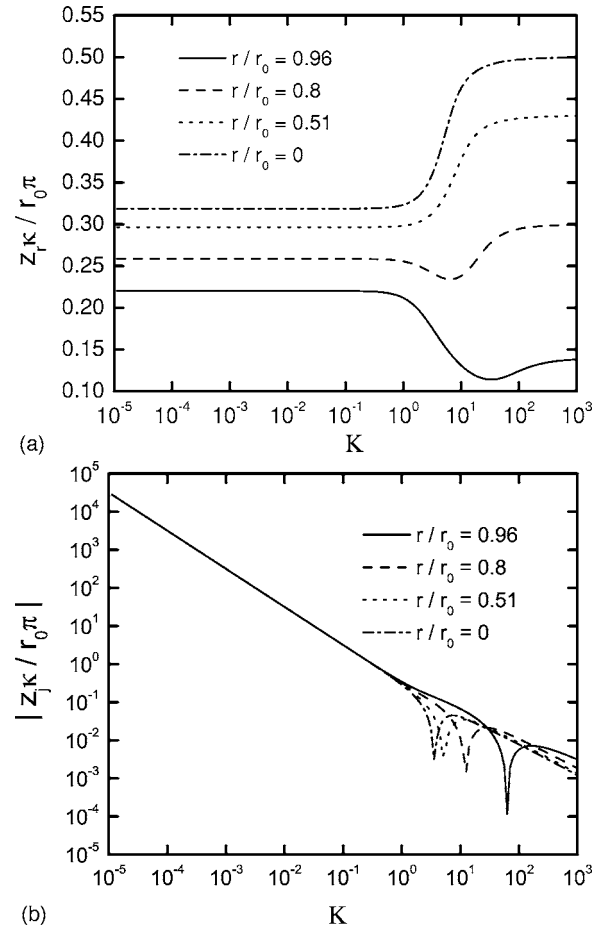
$$\frac{z_r \kappa}{r_0 \pi} \left(\frac{r}{r_0} \right) = 0.5 \sqrt{1 - \left(\frac{r}{r_0} \right)^2} \qquad [29]$$

derived from Eq. 1 using the expression for the primary resistance[1] in the form

$$R_e = \frac{1}{4\kappa r_0} \pi r_0^2 \qquad [30]$$

The radial distribution for the imaginary part of the impedance deviates from ideal capacitive behavior for frequencies $K > 1$.

Local ohmic impedance.— Following Eq. 23, the local ohmic impedance z_e accounts for the difference between the local interfacial and local impedances. As the local interfacial impedance corresponds to a pure capacitor, the term z_e cannot be a pure electrolyte resistance R_e. The calculated local ohmic impedance is presented in Fig. 11 in Nyquist format with radial position as a parameter. The shape of the diagrams are strongly dependent on the position on the electrode. At the periphery of the electrode, two time constants (inductive and capacitive loops) are seen, whereas at the electrode center only an inductive loop is evident. These loops are distributed around the asymptotic value of 1/4. The calculated values for real and imaginary parts of the local ohmic impedance are presented in Fig. 12a and b, respectively, as a function of frequency, with radial position as a parameter. The local ohmic impedance has only real values at $K \to 0$ and $K \to \infty$, but in the frequency range $10^{-2} < K < 100$, z_e has both real and imaginary components. Figure 12a clearly shows the asymptotic behavior in the low frequency range with values distributed around 1/4.

Global interfacial and global ohmic impedance.— The local interfacial impedance is associated with a pure capacitance that is independent of radial position. Thus, the global interfacial impedance arises from a pure capacitance C_0 in units of μF/cm^2. The global ohmic impedance Z_e is obtained from the global impedance Z by the expression

$$Z_e = Z - \frac{1}{jC_0\omega} \qquad [31]$$

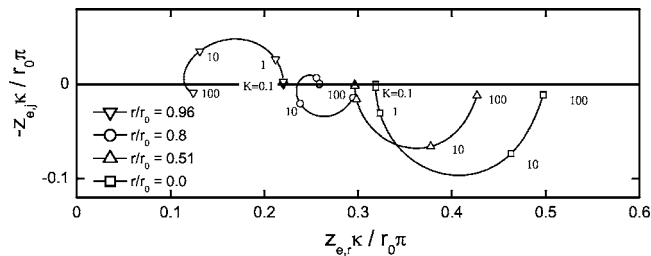or, in the dimensionless terms used in the present work
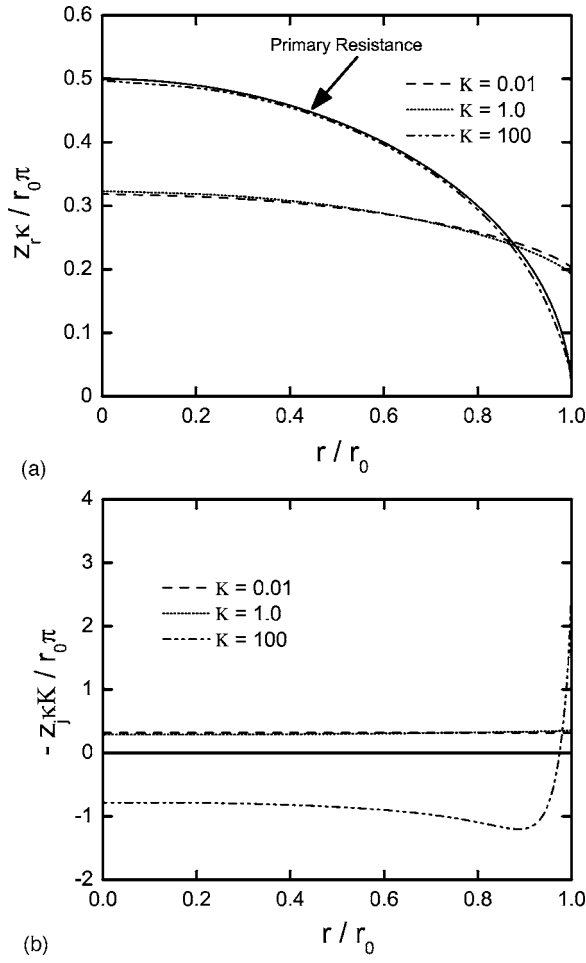
Figure 10. Calculated local impedance as a function of radial position: (a) real part and (b) imaginary part multiplied by dimensionless frequency K. The solid line is given in Fig. 10b to indicate the axis at $z_j = 0$.
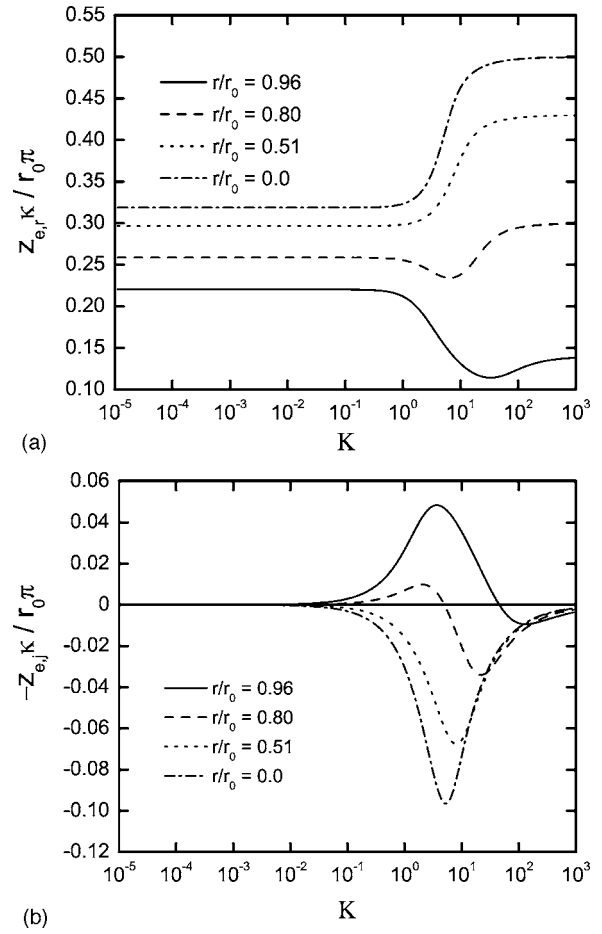

Figure 12. Calculated values for local ohmic impedance as a function of frequency with radial position as a parameter: (a) real part and (b) imaginary part. The solid line is given in Fig. 12b to indicate the axis at $z_{e,j} = 0$.

$$\frac{Z_e\kappa}{r_0\pi} = \frac{Z\kappa}{r_0\pi} - \frac{1}{j\pi K} \qquad [32]$$

The real part of Z_e is equal to the real part of Z as given in Fig. 4a. The imaginary part of Z_e is given in Fig. 13 as a function of dimensionless frequency K. In the low frequency range Z_e is a pure resistance equal to $1.08R_e$, and in the high frequency range Z_e tends towards R_e.

The imaginary part of the global ohmic impedance shows a non-zero value in the frequency range that is influenced by the current and potential distributions. Figures 4a and 13 show that all the effects of the current and potential distribution appears in the global ohmic impedance.

At high and low frequency limits, the global ohmic impedance defined in the present work is consistent with the accepted understanding of the ohmic resistance to current flow to a disk electrode. The global ohmic impedance approaches, at high frequencies, the primary resistance for a disk electrode (Eq. 30) described by

Figure 11. The local ohmic impedance in Nyquist format with radial position as a parameter.
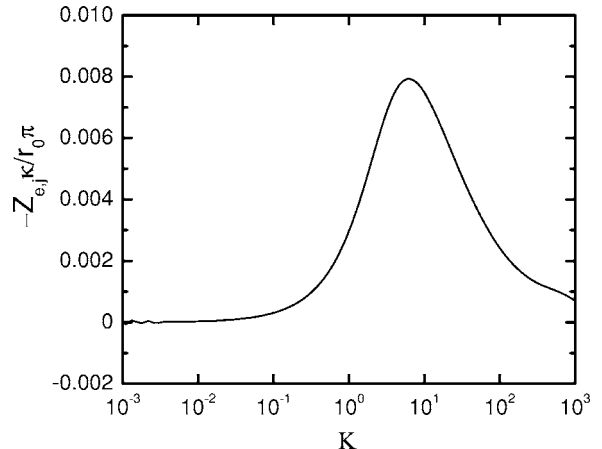
Figure 13. The imaginary part of the global ohmic impedance, calculated from Eq. 32, as a function of dimensionless frequency.

Newman.[1] The global ohmic impedance approaches, at low frequencies, the value for the ohmic resistance calculated by Newman[18] for a disk electrode.

The complex nature of both the global and local ohmic impedances is seen at intermediate frequencies. This complex value is the origin of the inductive features calculated for the local impedance and the quasi-CPE behavior found at high frequency for the global impedance.

Conclusions

The global impedance for an ideally polarized disk electrode is influenced by current and potential distributions at high frequencies. While the local interfacial impedance shows the expected ideally polarized behavior, the local impedance shows inductive behavior at high frequency and ideal behavior at low frequency. The local impedance is influenced by the local ohmic impedance, which has complex behavior near dimensionless frequency $K = 1$. The imaginary part of both the local and global ohmic impedance is equal to zero at both high and low frequencies where the ohmic impedance has purely resistive character.

The explanation of the frequency dispersion requires a coherent notation for local and global impedance which accounts for global, local, local interfacial, and both the local and global ohmic impedances. A notation is proposed in Table I that extends terms found in the local impedance literature to account for both local ohmic and local interfacial impedances.

The local and global ohmic impedance is shown to provide insight into the frequency dispersion associated with the geometry of disk electrodes. The high-frequency impedance response has the appearance of a CPE but can be considered to be only an apparent CPE because the CPE exponent α is not independent of frequency.

Acknowledgment

References

1. J. S. Newman, *J. Electrochem. Soc.*, **113**, 501 (1966).
2. J. S. Newman, *J. Electrochem. Soc.*, **113**, 1235 (1966).
3. K. Nisancioglu and J. Newman, *J. Electrochem. Soc.*, **120**, 1339 (1973).
4. K. Nisancioglu and J. Newman, *J. Electrochem. Soc.*, **121**, 523 (1974).
5. P. Antohi and D. A. Scherson, *J. Electrochem. Soc.*, **153**, E17 (2006).
6. K. B. Oldham, *Electrochem. Commun.*, **6**, 210 (2004).
7. G. J. Brug, A. L. G. van den Eeden, M. Sluyters-Rehbach, and J. H. Sluyters, *J. Electroanal. Chem. Interfacial Electrochem.*, **176**, 275 (1984).
8. J. R. Macdonald, *Impedance Spectroscopy: Emphasizing Solid Materials and Systems*, John Wiley & Sons, New York (1987).
9. A. Lasia, in *Modern Aspects of Electrochemistry*, Vol. 32 R. E. White, B. E. Conway, and J. O. Bockris, Editors, p. 143, Plenum Press, New York (1999).
10. Z. Lukacs, *J. Electroanal. Chem.*, **432**, 79 (1997).
11. Z. Lukacs, *J. Electroanal. Chem.*, **464**, 68 (1999).
12. J. R. Macdonald, *J. Appl. Phys.*, **58**, 1971 (1985).
13. J. R. Macdonald, *J. Appl. Phys.*, **58**, 1955 (1985).
14. R. L. Hurt and J. R. Macdonald, *Solid State Ionics*, **20**, 111 (1986).
15. J. R. Macdonald, *J. Appl. Phys.*, **62**, R51 (1987).
16. J. R. Macdonald, *J. Electroanal. Chem.*, **378**, 17 (1994).
17. J.-B. Jorcin, M. E. Orazem, N. Pébère, and B. Tribollet, *Electrochim. Acta*, **51**, 1473 (2006).
18. J. S. Newman, *J. Electrochem. Soc.*, **117**, 198 (1970).
19. V. M.-W. Huang, V. Vivier, I. Frateur, M. E. Orazem, and B. Tribollet, *J. Electrochem. Soc.*, **154**, C89 (2006).
20. V. M.-W. Huang, V. Vivier, M. E. Orazem, N. Pébère, and B. Tribollet, *J. Electrochem. Soc.*, **154**, C99 (2006).
21. L. Young, *Trans. Faraday Soc.*, **51**, 1250 (1955).
22. L. Young, *Anodic Oxide Films*, Academic Press, New York (1961).
23. C. A. Schiller and W. Strunz, *Electrochim. Acta*, **46**, 3619 (2001).
24. R. Jurczakowski, C. Hitz, and A. Lasia, *J. Electroanal. Chem.*, **572**, 355 (2004).
25. T. Pajkossy, *Solid State Ionics*, **176**, 1997 (2005).
26. G. Sewell, *The Numerical Solution of Ordinary and Partial Differential Equations*, John Wiley & Sons, New York (2005).
27. R. S. Lillard, P. J. Moran, and H. S. Isaacs, *J. Electrochem. Soc.*, **139**, 1007 (1992).
28. F. Zou, D. Thierry, and H. S. Isaacs, *J. Electrochem. Soc.*, **144**, 1957 (1997).
29. M. E. Orazem, N. Pébère, and B. Tribollet, *J. Electrochem. Soc.*, **153**, B129 (2006).